

$S = 2$ quasi-one-dimensional spin waves in CrCl_2

M. B. Stone, G. Ehlers, and G. E. Granroth

Quantum Condensed Matter Science Division, Oak Ridge National Laboratory, Oak Ridge, Tennessee 37831, USA

(Received 11 June 2013; revised manuscript received 29 August 2013; published 16 September 2013)

We examine the magnetic excitation spectrum in the $S = 2$ Heisenberg antiferromagnet CrCl_2 . Inelastic neutron scattering measurements on powder samples are able to determine the significant exchange interactions in this system. A large anisotropy gap is observed in the spectrum below the Néel temperature and the ratio of the two largest exchange constants is $J_c/J_b = 9.1 \pm 2.2$. However, no sign of a gapped quantum spin liquid excitation was found in the paramagnetic phase.

DOI: [10.1103/PhysRevB.88.104413](https://doi.org/10.1103/PhysRevB.88.104413)

PACS number(s): 75.50.Ee, 78.70.Nx, 75.10.Pq

I. INTRODUCTION

Haldane's 1983 conjecture of massive excitations from a disordered ground state in 1D Heisenberg integer spin, S , antiferromagnets spurred experimental physics into action.^{1,2} In addition to analytic and numerical calculations, the spectra and thermodynamic signatures of experimental systems were pursued with rigor.³⁻⁸ The magnetic excitation spectrum with a spin-gap of $\Delta \approx 0.41J$,⁹ where J is the nearest-neighbor exchange constant, has also been clearly observed using inelastic neutron scattering techniques for several systems.¹⁰⁻¹² While $S = 1$, one-dimensional antiferromagnets have made up the core of such studies; $S > 1$ integer spin compounds have not been as forthcoming.

The spin-gap for $S = 2$ has been calculated to be approximately $\Delta \approx 0.087J$.^{13,14} This reduced energy scale makes experimental studies of the physics associated with the disordered ground state difficult. Furthermore, the disordered gapped phase (i.e., Haldane phase) portion of the phase diagram as a function of Ising and single-ion anisotropy becomes smaller and smaller as the spin quanta increases.¹³ This further limits the possibility of experimental systems supporting an Haldane phase for $S > 1$. The $S = 2$ quasi-one-dimensional antiferromagnet CsCrCl_3 , with an ordering temperature of $T_N \approx 16$ K, has been examined;¹⁵ however, measurements in the disordered phase ($T > T_N$) imply the system is not in the Haldane phase.^{16,17} There are only several other systems examined in terms of quasi-one-dimensional $S = 2$ chains, including $\text{MnCl}_3(\text{bipy})$,^{18,19} $\alpha\text{-NaMnO}_2$,²⁰ $\text{FePb}_4\text{Sb}_6\text{S}_{14}$,^{21,22} and *catena*- $\text{MnF}(\text{salen})$.²³

There has been great success in probing quantum fluctuations associated with quasi-one-dimensional connectivity in real-world experimental systems that ultimately order magnetically.²⁴⁻²⁸ Further motivated by the general lack of $S = 2$ quasi-one-dimensional antiferromagnets and the potential to directly measure the excitation spectrum of a Haldane gap phase for $S = 2$, we have chosen to examine CrCl_2 . This system has previously been proposed to be an $S = 2$ low-dimensional antiferromagnet.^{29,30} Although initial characterization was made some time ago, no spectroscopic investigations have been performed until now. Magnetic susceptibility measurements have considered CrCl_2 to be a $S = 2$ antiferromagnetic (AFM) chain with $J = 19$ K (1.6 meV) with $T_N \approx 20$ K.^{29,31} The fact that this system exhibits magnetic order immediately invalidates the possibility of a low-temperature disordered magnetic ground state, and

therefore any gap in the excitation spectrum for $T < T_N$ would not be a so-called Haldane gap. Above T_N , the ground state is disordered and may be highly influenced by quantum fluctuations associated with any one- or two-dimensional magnetic interactions. It is very difficult, however, to determine the exchange connectivity conclusively from thermodynamic measurements alone. We examine the potential quasi-1D, $S = 2$ antiferromagnet CrCl_2 using inelastic neutron scattering measurements. Through a comparison of the measured spectra to linear spin-wave theory, we are able to deduce the significant exchange couplings and single ion anisotropy in this compound. From these measurements, we conclude that the system is better described by a classical spin wave model.

Recent density functional theory calculations predict that CrCl_2 is a quasi-1D Heisenberg antiferromagnet with the greatest exchange along the c axis between the Cr^{2+} sites.³⁰ Including onsite Coulomb repulsion in these calculations yields a 1D exchange of $J = 19.2$ K with a net ferromagnetic interchain exchange of $J' = -2.92$ K, very similar to the values found in analysis of the magnetic susceptibility data. The nuclear structure of CrCl_2 (orthorhombic $Pnmm$) is shown in Fig. 1.³²⁻³⁴ Room temperature lattice constants are reported as $a = 6.64(1)$, $b = 5.98(1)$, and $c = 3.48(1)$ Å,^{32,35} making the nearest-neighbor Cr-Cr distance 3.48(1) Å along the c axis. The Cr ions reside in the center of a distorted octahedron of Cl ions as shown in Fig. 1. The Cr^{2+} ions are coplanar with the four Cl ions, which make up the base of the bipyrimids of the octahedron. These planes are in turn coplanar with neighbors along the c axis. Early neutron diffraction measurements found $T_N \approx 20$ K with a doubling of the b and c axes in the ordered antiferromagnetic phase where the ordered moments point parallel to the long Cr-Cl bonds of the octahedra.³³ Figure 1 illustrates the periodicity of the ordered moments in the crystal structure.

II. EXPERIMENTAL METHODS

Inelastic neutron scattering measurements were performed on a sample of approximately 5 g of CrCl_2 powder (Alfa Aesar 99.9%) in a cylindrical aluminum sample can with helium exchange gas. Sample loading took place within a helium glove box to reduce any contamination with atmospheric water. CrCl_2 is very hygroscopic.³² Neutron scattering measurements were performed using the ARCS,³⁶ SEQUOIA,³⁷ and CNCS³⁸ direct geometry chopper spectrometers at the Spallation Neutron Source at the Oak Ridge National Laboratory. The sample

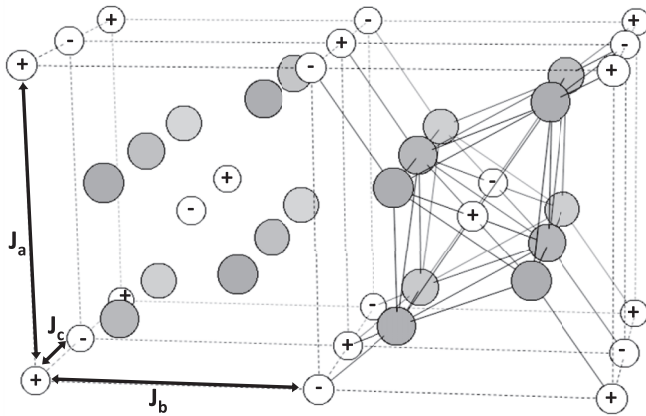


FIG. 1. Nuclear and magnetic structure of CrCl_2 .^{32,33} Open circles represent Cr atomic sites and gray circles represent Cl atomic sites. Proposed exchange constants along the a , b , and c directions are illustrated with arrows in the left unit cell. Cr-Cl and Cl-Cl bonding are shown on the right side of the figure. The phase of the ordered moments on the Cr sites is shown using $+$ and $-$ symbols. Dashed lines correspond to the nuclear unit cell.

was attached to the cold-finger of a bottom-loading closed-cycle refrigerator for the ARCS and SEQUOIA measurements. The sample was within a liquid helium flow cryostat for the CNCS measurement. The ARCS/SEQUOIA measurements were made using a ferri chopper phase for an incident energy of $E_i = 15$ meV and spinning a 100-mm-long slit package with 1.5/2.0-mm-wide slats at 180/240 Hz. The CNCS measurement was performed in the high-flux configuration of the instrument with $E_i = 4.2$ meV.

III. RESULTS AND DISCUSSION

Figure 2 shows the inelastic measurements from the (a) ARCS, (b) SEQUOIA, and (c) CNCS instruments. There is a clear excitation centered at approximately 4 meV energy transfer, $\hbar\omega$, with an energy gap of ≈ 2 meV. The rapid fall-off in scattering intensity with increasing wave-vector transfer, Q , indicates that the scattering is magnetic in origin. Though the measurement is *powder averaged* one can see underlying dispersion in the data in Fig. 2(b). There also appears to be a flat mode at approximately 2.5 meV energy transfer. This suggests a singularity in the magnetic density of states as typically found in one-dimensional antiferromagnets.^{39,40} As we discuss later in the manuscript, this feature is a manifestation of the powder averaged quasi-one-dimensional spin-wave spectrum. The CNCS measurement Fig. 2(c) allows one to place limits on the value of the energy gap as a function of temperature with good energy resolution. In the ordered phase, at $T = 5$ K, the gap is very well defined as 2.1(1) meV.

Figure 3 shows diffraction measurements of CrCl_2 as measured using the CNCS spectrometer with $E_i = 4.2$ meV. Figure 3(a) shows the integrated scattering intensity for four temperatures. There are clear magnetic Bragg peaks located at $Q = 1.06$ and 1.42 \AA^{-1} that appear below the ordering temperature. In Fig. 3(b), one can see that above T_N there is also an increase in the diffuse scattering intensity over a range of wave-vector transfer. This increase is critical scattering

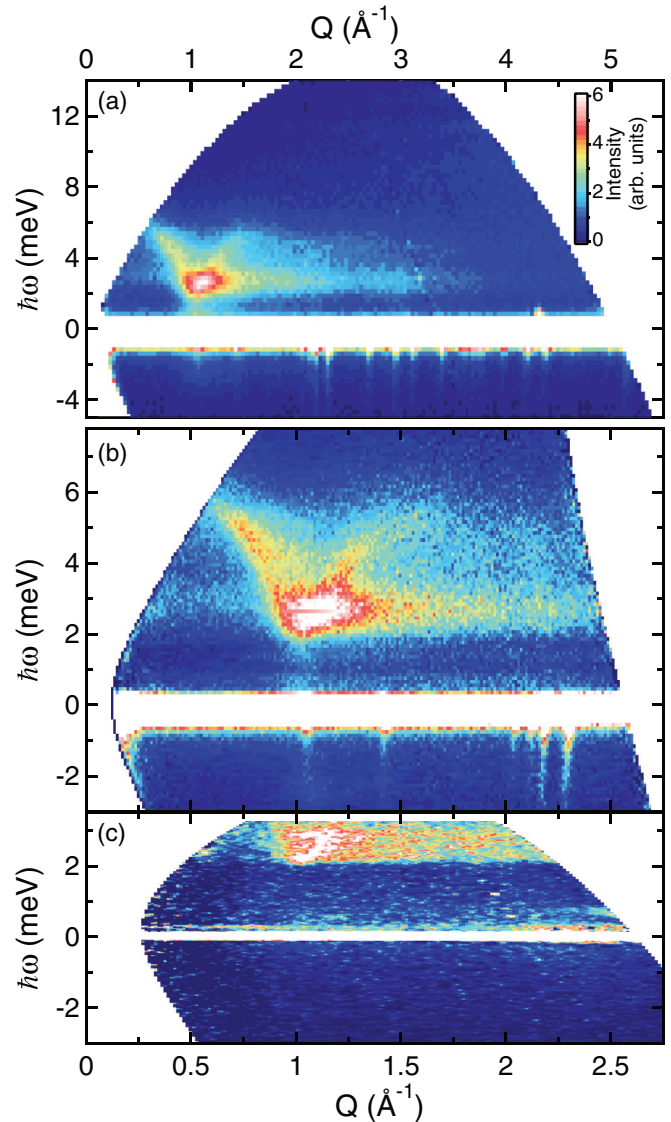


FIG. 2. (Color online) Inelastic scattering intensity as a function of energy and wave-vector transfer for CrCl_2 . Measurements were made at $T = 5$ K. (a) Data from ARCS measured with $E_i = 15$ meV. Top axis corresponds to wave-vector transfer. (b) Data from SEQUOIA measured with $E_i = 15$ meV. Bottom axis corresponds to wave-vector transfer. (c) Data from CNCS measured with $E_i = 4.2$ meV. Bottom axis corresponds to wave-vector transfer. Data in (c) have been background subtracted using an empty aluminum sample can measurement.

associated with integrating over the magnetic fluctuations. The location of the first magnetic Bragg peak corresponds well to the large density of states of the inelastic spectrum shown in Fig. 2 at 2 meV and $Q \approx 1 \text{ \AA}^{-1}$.

The peak at $Q = 1.42 \text{ \AA}^{-1}$ in Fig. 3(a) is the (110) nuclear Bragg peak of CrCl_2 . However, the small peaks at $Q = 1.72$ and 1.14 \AA^{-1} can be indexed to a small contribution from the hydrate of the parent compound $\text{CrCl}_2 \cdot 8(\text{H}_2\text{O})$: (020) and (011), respectively. The magnetic peak at $Q = 1.06 \text{ \AA}^{-1}$ and $Q = 1.42 \text{ \AA}^{-1}$ index well as $(0\frac{1}{2}\frac{1}{2})$ and $(1\frac{1}{2}\frac{1}{2})$ antiferromagnetic Bragg peaks.

Measurements were made as a function of warming and cooling of the sample. Figure 3(c) illustrates the extracted peak

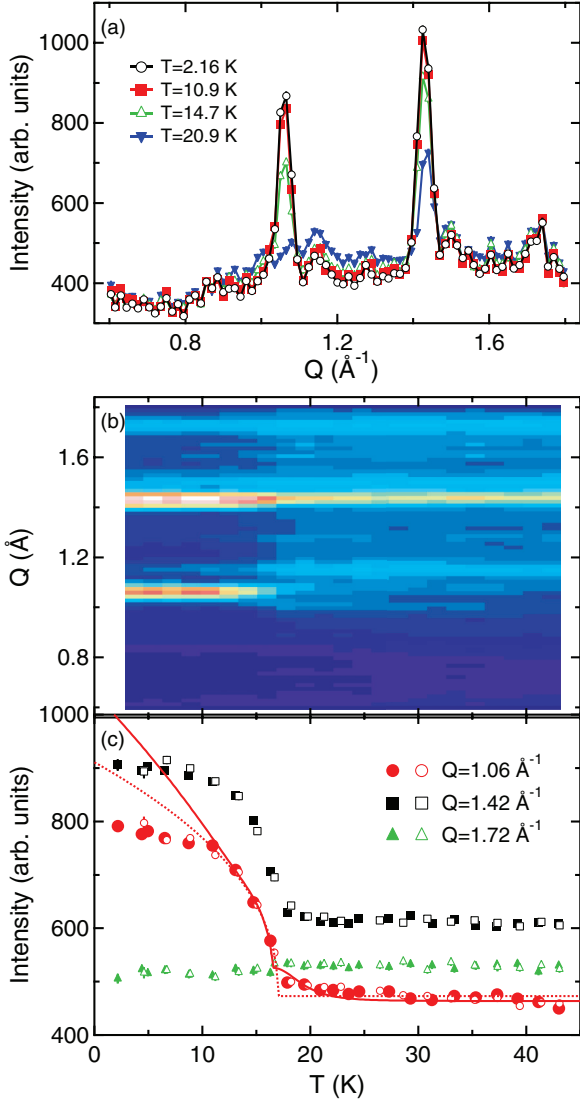


FIG. 3. (Color online) Neutron diffraction measurements of CrCl_2 as a function of temperature. Measurements are from the CNCS spectrometer for $E_i = 4.2$ meV integrated between -4 and 4 meV energy transfer. Data have been background subtracted using an empty aluminum sample can measurement. (a) Scattering intensity at four select temperatures. (b) Temperature- and wave-vector-dependent scattering intensity for warming the sample. (c) Integrated scattering intensity for warming (solid symbols) and cooling (open symbols). Data have been integrated with a total width in wave-vector transfer of $\Delta Q = 0.04 \text{ \AA}^{-1}$. Solid and dotted lines correspond to power-law fits between 13 and 43 K as described in the text.

intensity for warming and cooling for nuclear and magnetic Bragg peaks. There is no hysteresis in the magnetic ordering, and we observe no significant change in nuclear structure as a function of temperature that may be associated with a structural phase transition. We simultaneously fit the $Q = 1.06$ and 1.42 \AA^{-1} using a power-law with an additional Lorentzian function centered at T_N to account for the critical scattering,

$$I = A + B(T_N - T)^{2\beta} + \frac{C}{[(T - T_N)^2 + \Gamma^2]^2}, \quad (1)$$

where the constant background A was fixed to the average scattering intensity for $T > 35$ K. This fit result (reduced

$\chi^2 = 6.08$) is shown as a solid line in Fig. 3(c), where $\beta = 0.31(4)$ and $T_N = 16.5(1)$ K. We also fit these data to a single power law (Eq. (1) with $C = 0$) allowing the constant A to vary. The resulting fit (reduced $\chi^2 = 6.83$) is shown as a dotted line in Fig. 3(c) with values of $\beta = 0.22(3)$ and $T_N = 17.0(2)$ K. The critical exponent β for both characterizations of the magnetic order parameter is reduced from the 3D Heisenberg value implying $d < 3$ interactions, although more precise measurements would be able to make this classification more robust.⁴¹

We use linear spin wave theory (LSWT) to calculate a dispersion, $\hbar\omega(\mathbf{Q})_{\text{sw}}$, for comparison to the measured data. The local environment of the magnetic ion, the direction of the ordered moments, and the gap in the AFM spectrum imply the need for an anisotropy parameter, D . The Heisenberg Hamiltonian with a single-ion anisotropy parameter, D , is

$$\mathcal{H} = \sum_{\alpha} \sum_{\langle ij \rangle_{\alpha}} J_{\alpha} \mathbf{S}_i \cdot \mathbf{S}_j + \sum_i D(S_z^2)_i, \quad (2)$$

where α is summed over a, b , and c , and we define the z axis to be along the ordered moment.^{42,43} For the ordered structure

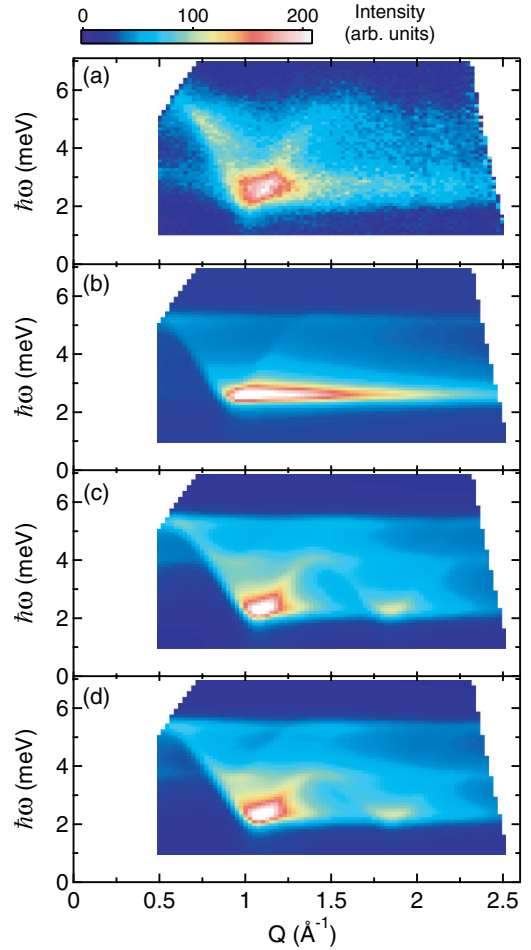


FIG. 4. (Color online) (a) Image plot of the scattering intensity as a function of energy and wave-vector transfer for CrCl_2 at $T = 5$ K as measured using the SEQUOIA instrument. (b) Calculated scattering intensity including J_c and D fitting parameters as described in the text. (c) Calculated scattering intensity including J_c , D , and J_b fitting parameters as described in the text. (d) Calculated scattering intensity including J_c , D , J_b , and J_a fitting parameters as described in the text.

shown in Fig. 1, this results in the spin-wave dispersion

$$\begin{aligned} A_{\mathbf{Q}} &= 2S\{J_a[\cos(2\pi H) - 1] + J_b + J_c + D\} \\ B_{\mathbf{Q}} &= 2S[J_b \cos(2\pi K) + J_c \cos(2\pi L)] \\ \hbar\omega(\mathbf{Q})_{\text{SW}} &= \sqrt{A_{\mathbf{Q}}^2 - B_{\mathbf{Q}}^2}, \end{aligned} \quad (3)$$

where S is the magnitude of the spin quantum and the exchange interactions are illustrated in Fig. 1.⁴⁴ Although a single crystal measurement is preferential, comparison of the powder averaged scattering intensity is able to determine the significant exchange interactions.⁴⁵ We fit our measured low-temperature spectrum, Fig. 4, by comparing it to a numerically powder averaged LSWT scattering intensity for the dispersion given in Eq. (2).⁴² The calculated scattering intensity was convolved with a Lorentzian function with a width Γ . Each spectra was also convolved with the mean instrumental energy and wave-vector resolution function over the range of data shown in Fig. 4. For each calculation, the value of Γ was fixed to 0.1 meV. This value is reasonable given the width of inelastic features in the spectrum shown in Fig. 4(a). We examine spectra by first including only the most dominant terms in the Hamiltonian. Each calculated spectra was fit to the measured spectrum using an overall multiplicative prefactor and a constant additive background. The value of the parameter that minimized the reduced value of χ^2 was used as the starting value for the iteration over the next parameter in the Hamiltonian.⁴⁶ This process was repeated until the χ^2 minimum no longer changed. The error bars in the exchange parameters are determined by the value where the reduced χ^2 increases by one above its minimum value. Figure 4(b) shows the fitted spectrum when including only the D and J_c parameters with $J_c = 1.16 \pm 0.15$, $D = 0.161^{+0.030}_{-0.026}$ meV, and $\chi^2 = 7.67$. This simple one-dimensional model agrees well with the gap and bandwidth in the measured spectrum. Including the J_b exchange constant further improves the fit, $\chi^2 = 3.67$, Fig. 4(c). The fitted exchange constants for this fit do not vary significantly from those used in Fig. 4(b): $J_c = 1.06 \pm 0.11$, $D = 0.11 \pm 0.02$, and $J_b = 0.170^{+0.065}_{-0.080}$ meV. Adding the J_b parameter introduces additional localization of scattering intensity throughout the spectrum. For example, one can see an additional portion of the spectrum has developed below $Q = 1 \text{ \AA}^{-1}$ between 4 and 5 meV energy transfer. Including the J_a parameter marginally improves the fit, $\chi^2 = 3.66$, as shown in Fig. 4(d), with small changes in the exchange constants: $J_c = 1.13^{+0.13}_{-0.12}$, $D = 0.11 \pm 0.02$, $J_b = 0.12 \pm 0.07$ meV, and $J_a = -0.001 \pm 0.02$ meV. The J_a value is ferromagnetic in agreement with the determined magnetic structure, but it is very small in comparison to recent DFT calculations.³⁰ The primary exchange value agrees fairly well with those used to describe the higher-temperature magnetic susceptibility data as well as those from DFT calculations. It was originally proposed from magnetic susceptibility measurements of CrCl_2 and the magnetic transition temperature that the ratio of intrachain to interchain interactions would be of the order of 5×10^{-2} .^{47,48} This value is very close to the ratio of the mean interchain to intrachain interaction value we have determined: $\frac{J_a + J_b}{2} \frac{1}{J_c} = 0.05 \pm 0.02$. These exchange parameters describe a gapped excitation that is highly dispersive along the b and c axes with a gap of 2.1 meV and a total bandwidth of 3.3 meV.

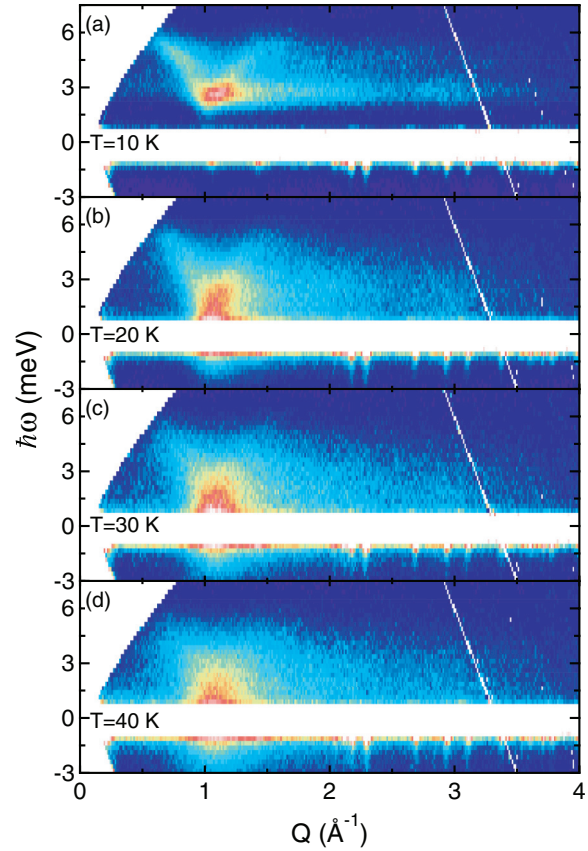


FIG. 5. (Color online) Energy- and wave-vector-dependent scattering intensity for CrCl_2 at four temperatures. Data were measured using the ARCS instrument.

The intensity distribution is in fairly good agreement with our measurement. No significant contribution for interactions along the (111) direction, J_{111} , could be determined based upon our powder measurements. Single-crystal measurements may be able to determine the current exchange constants more precisely and may determine weaker exchange constants. These would likely serve to fill in additional scattering intensity in the model in the vicinity of 2.5 meV energy transfer for $Q > 1.25 \text{ \AA}^{-1}$.

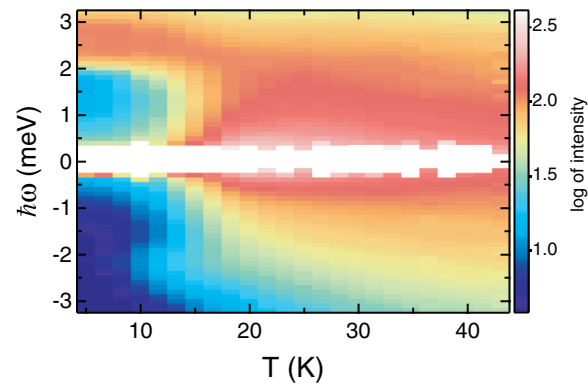


FIG. 6. (Color online) Energy-dependent scattering intensity for CrCl_2 as a function of temperature. Data were integrated between 0.9 and 1.2 inverse angstroms in wave-vector transfer. Data were measured using the CNCS instrument.

Given the primary exchange constant, $J_c = 1.13_{-0.12}^{+0.13}$ meV, the Haldane gap energy for CrCl₂ would be on the order of 0.1 meV. Any potential quantum fluctuations for $T > T_N$ would be obscured by thermal effects. Figure 5 shows the temperature-dependent spectrum for CrCl₂ for temperatures below and above T_N . As the temperature increases the anisotropy gap in the spectrum closes and the scattering intensity begins to shift toward $\hbar\omega = 0$ and $Q = 0$. Finer resolution measurements as a function of temperature are shown in Fig. 6. This figure is composed of a series of constant wave vector scans integrated between 0.9 and 1.2 inverse angstroms. The data are plotted as the logarithm of the scattering intensity to help illustrate differences in the scattering intensity near $\hbar\omega = 0$. As the temperature is increased, the spin-wave excitation dampens and moves to lower energy transfer. The fluctuations above T_N appear to be paramagnetic with no sign of a quantum spin gap.

IV. CONCLUSIONS

The spectrum and the determined exchange constants for CrCl₂ serve to classify this system as a $S = 2$ quasi-one-

dimensional antiferromagnet. The ratio of the two largest exchange constants is only $J_c/J_b \approx 9.1$ and there exists a significant onsite anisotropy contributing to the energy gap in the low-temperature spin wave spectrum. The anisotropic exchange constants are in the vicinity of recent DFT calculations lending additional credence to the respective band structure calculations.³⁰ We also find no sign of a Haldane gap in the paramagnetic phase. Single-crystal inelastic neutron scattering measurements in the vicinity of the antiferromagnetic wave-vector with exceptional energy resolution may be able to place additional limits on the existence of such quantum fluctuations in CrCl₂.

ACKNOWLEDGMENTS

The research was performed at Oak Ridge National Laboratory's Spallation Neutron Source and was sponsored by the Scientific User Facilities Division, Office of Basic Energy Sciences, US Department of Energy. We are grateful for stimulating discussions with M. W. Meisel and I. Zaliznyak.

-
- ¹F. D. M. Haldane, *Phys. Rev. Lett.* **50**, 1153 (1983).
²F. D. M. Haldane, *Phys. Lett. A* **93**, 464 (1983).
³J. B. Parkinson, J. C. Bonner, G. Müller, M. P. Nightingale, and H. W. J. Blöte, *J. Appl. Phys.* **57**, 3319 (1985).
⁴J. B. Parkinson and J. C. Bonner, *Phys. Rev. B* **32**, 4703 (1985).
⁵I. Affleck, *Phys. Rev. Lett.* **54**, 966 (1985).
⁶W. J. L. Buyers, R. M. Morra, R. L. Armstrong, M. J. Hogan, P. Gerlach, and K. Hirakawa, *Phys. Rev. Lett.* **56**, 371 (1986).
⁷H. J. Schulz, *Phys. Rev. B* **34**, 6372 (1986).
⁸M. Steiner, K. Kakurai, J. K. Kjems, D. Petitgrand, and R. Pynn, *J. Appl. Phys.* **61**, 3953 (1987).
⁹S. V. Meshkov, *Phys. Rev. B* **48**, 6167 (1993).
¹⁰S. Ma, C. Broholm, D. H. Reich, B. J. Sternlieb, and R. W. Erwin, *Phys. Rev. Lett.* **69**, 3571 (1992).
¹¹I. A. Zaliznyak, S. H. Lee, and S. V. Petrov, *Phys. Rev. Lett.* **87**, 017202 (2001).
¹²A. Zheludev, Y. Chen, C. L. Broholm, Z. Honda, and K. Katsumata, *Phys. Rev. B* **63**, 104410 (2001).
¹³U. Schollwöck and T. Jolicœur, *Europhys. Lett.* **30**, 493 (1995).
¹⁴X. Wang, S. Qin, and L. Yu, *Phys. Rev. B* **60**, 14529 (1999).
¹⁵Y. Tazuke, H. Tanaka, K. Iio, and K. Nagata, *J. Phys. Soc. Jpn.* **53**, 3191 (1984).
¹⁶S. Itoh, H. Tanaka, and T. Otomo, *J. Phys. Soc. Jpn.* **66**, 455 (1997).
¹⁷S. Itoh, H. Tanaka, and M. J. Bull, *J. Phys. Soc. Jpn.* **71**, 1148 (2002).
¹⁸G. E. Granroth, M. W. Meisel, M. Chaparala, Th. Jolicœur, B. H. Ward, and D. R. Talham, *Phys. Rev. Lett.* **77**, 1616 (1996).
¹⁹G. E. Granroth, Ph.D. dissertation, University of Florida, 1998.
²⁰C. Stock, L. C. Chapon, O. Adamopoulos, A. Lappas, M. Giot, J. W. Taylor, M. A. Green, C. M. Brown, and P. G. Radaelli, *Phys. Rev. Lett.* **103**, 077202 (2009).
²¹P. Léone, G. André, C. Doussier, and Y. Moëlo, *J. Magn. Magn. Mater.* **284**, 92 (2004).
²²Y. Matsushita and Y. Ueda, *Inorg. Chem.* **42**, 7830 (2003).
²³T. Birk, K. S. Pedersen, S. Piligkos, C. Aa. Thuesen, H. Weihe, and J. Bendix, *Inorg. Chem.* **50**, 5312 (2011).
²⁴M. B. Stone, W. Tian, M. D. Lumsden, G. E. Granroth, D. Mandrus, J.-H. Chung, N. Harrison, and S. E. Nagler, *Phys. Rev. Lett.* **99**, 087204 (2007).
²⁵I. A. Zaliznyak, L.-P. Regnault, and D. Petitgrand, *Phys. Rev. B* **50**, 15824 (1994).
²⁶M. Kenzelmann, R. A. Cowley, W. J. L. Buyers, and D. F. McMorrow, *Phys. Rev. B* **63**, 134417 (2001).
²⁷B. Lake, D. A. Tennant, C. D. Frost, and S. E. Nagler, *Nat. Mater.* **4**, 329 (2005).
²⁸D. A. Tennant, R. A. Cowley, S. E. Nagler, and A. M. Tsvetlik, *Phys. Rev. B* **52**, 13368 (1995).
²⁹M. Hagiwara and K. Katsumata, *J. Magn. Magn. Mater.* **140-144**, 1665 (1995).
³⁰A. Hermann, B. Vest, and P. Schwerdtfeger, *Phys. Rev. B* **74**, 224402 (2006).
³¹The values in Ref. 29 are $J = 9.5$ K (0.82 meV) for a numerical calculation with five spins. These values most likely correspond to a Hamiltonian with $2J \sum_{i=1}^n \mathbf{S}_i \cdot \mathbf{S}_{i+1}$.
³²J. W. Tracy, N. W. Gregory, E. C. Lingafelter, J. D. Dunitz, H.-C. Mez, R. E. Rundle, C. Scheringer, H. L. Yakel, Jr., and M. K. Wilkinson, *Acta Crystallogr.* **14**, 927 (1961).
³³J. W. Cable, M. K. Wilkinson, and E. O. Wollan, *Phys. Rev.* **118**, 950 (1960).
³⁴H. R. Oswald, *Helv. Chim. Acta* **44**, 1049 (1961).
³⁵Unless otherwise noted, values in parentheses represent one standard deviation, and error bars shown in figures represent one standard deviation.
³⁶D. L. Abernathy, M. B. Stone, M. J. Loguillo, M. S. Lucas, O. Delaire, X. Tang, J. Y. Y. Lin, and B. Fultz, *Rev. Sci. Instrum.* **83**, 15114 (2012).

- ³⁷G. E. Granroth, A. I. Kolesnikov, T. E. Sherline, J. P. Clancy, K. A. Ross, J. P. C. Ruff, B. D. Gaulin, and S. E. Nagler, *J. Phys.: Conf. Ser.* **251**, 12058 (2010).
- ³⁸G. Ehlers, A. A. Podlesnyak, J. L. Niedziela, E. B. Iverson, and P. E. Sokol, *Rev. Sci. Instrum.* **82**, 85108 (2011).
- ³⁹U. Schollwöck, J. Richter, D. J. J. Farnell, and R. F. Bishop (eds.), *Quantum Magnetism* (Springer-Verlag, Berlin, Germany, 2004).
- ⁴⁰P. R. Hammar, D. H. Reich, C. Broholm, and F. Trouw, *Phys. Rev. B* **57**, 7846 (1998).
- ⁴¹J. C. Le Guillou and J. Zinn-Justin, *Phys. Rev. Lett.* **39**, 95 (1977).
- ⁴²S. W. Lovesey, *Theory of Neutron Scattering from Condensed Matter: Volume 2* (Clarendon Press, Oxford, UK, 1987).
- ⁴³P. A. Lindgård, A. Kowalska, and P. Laut, *J. Phys. Chem. Solids* **28**, 1357 (1967).
- ⁴⁴M. B. Stone, M. D. Lumsden, S. E. Nagler, D. J. Singh, J. He, B. C. Sales, and D. Mandrus, *Phys. Rev. Lett.* **108**, 167202 (2012).
- ⁴⁵M. B. Stone, M. D. Lumsden, Y. Qiu, E. C. Samulon, C. D. Batista, and I. R. Fisher, *Phys. Rev. B* **77**, 134406 (2008).
- ⁴⁶P. Bevington, *Data Reduction and Error Analysis for the Physical Sciences* (McGraw-Hill, New York, NY, 2003).
- ⁴⁷L. J. deJongh and A. R. Miedema, *Adv. Phys.* **23**, 1 (1974).
- ⁴⁸J. W. Stout and R. C. Chisholm, *J. Chem. Phys.* **36**, 979 (1962).